Available online at www.sciencedirect.com
ScienceDirect
Journal of Power Sources 163 (2007) 853–863
JOURNAL OF POWER SOURCES
www.elsevier.com/locate/jpowsour

An experimental and numerical investigation on the cross flow through gas diffusion layer in a PEM fuel cell with a serpentine flow channel

Jaewan Park, Xianguo Li *

Department of Mechanical Engineering, University of Waterloo, 200 University Ave W., Waterloo, Ontario, Canada N2L 3G1

Received 20 July 2006; received in revised form 21 September 2006; accepted 27 September 2006
Available online 13 November 2006

Abstract

A serpentine flow channel is one of the most common and practical channel layouts for a polymer electrolyte membrane (PEM) fuel cell since it ensures the removal of water produced in a cell with acceptable parasitic load. During the reactant flows along the flow channel, it can also leak or cross to neighboring channel via the porous gas diffusion layer due to the high pressure gradient caused by the short distance. Such a cross flow leads to a larger effective flow area altering reactant flow in the flow channel so that the resultant pressure and flow distributions are substantially different from that without considering cross flow, even though this cross flow has largely been ignored in previous studies. In this work, a numerical and experimental study has been carried out to investigate the cross flow in a PEM fuel cell. Experimental measurements revealed that the pressure drop in a PEM fuel cell is significantly lower than that without cross flow. Three-dimensional numerical simulation has been performed for wide ranges of flow rate, permeability and thickness of gas diffusion layer to analyze the effects of those parameters on the resultant cross flow and the pressure drop of the reactant streams. Considerable amount of cross flow through gas diffusion layer has been found in flow simulation and its effect on pressure drop becomes more significant as the permeability and the thickness of gas diffusion layer are increased. The effects of this phenomenon are also crucial for effective water removal from the porous electrode structure and for estimating pumping energy requirement in a PEM fuel cell, it cannot be neglected for the analysis, simulation, design, operation and performance optimization of practical PEM fuel cells.

Keywords: PEM fuel cell; Cross flow; Permeability; Serpentine flow channel; Numerical simulation; Experimental measurement

1. Introduction

Use of fossil fuels and consequent damage to the atmosphere has become one of the most serious concerns of modern times, and has called for environmentally friendly energy conversion and power generation systems for sustainable development. Polymer electrolyte membrane (PEM) fuel cells are a clean power source, at least at the point of use, and have been regarded as one of the most promising advanced energy technologies. Significant effort is being spent worldwide to develop PEM fuel cells for mobile, portable and stationary applications.

The performance of a PEM fuel cell is influenced immensely by the flow distributions in the flow channels and gas diffusion layer (GDL) since water flooding and concentration distribution are the most important issues governed by the configurations of flow channel layouts. Watkins et al. [1] proposed a continuous fluid flow channel that had an inlet at one end and an outlet at the other, and typically followed a serpentine path. Such a serpentine flow channel layout can be regarded as many parallel flow channels being connected in series. This flow channel design results in a long reactant flow path; consequently, a significant pressure drop occurs with considerable concentration gradients from the channel inlet to the outlet. Hence several separate flow channels are often adopted for large cells in order to reduce the pressure drop and excessive power requirement for the supply of air stream [2]. Classifications and details of discussions on flow field designs can be found in Li [3] and Li and Sabir [4].

Serpentine flow channel layout and many of its modifications are widely chosen as flow channel designs for PEM fuel cells owing to the fact that this flow channel design ensures effective water removal from the cell, while with reasonable pressure

* Corresponding author.
E-mail addresses: jwpark@engmail.uwaterloo.ca (J. Park), x6li@uwaterloo.ca (X. Li).

0378-7753/$ – see front matter © 2006 Elsevier B.V. All rights reserved.
doi:10.1016/j.jpowsour.2006.09.083

Nomenclature

A_{cell}	active cell area
C_f	wall friction coefficient
C_l	a constant in the expression for the laminar wall friction coefficient
d	flow channel depth (m)
d_h	flow channel hydraulic diameter (m)
F	Faraday constant
H	bipolar plate effective height (m)
J	cell current density ($A\,cm^{-2}$)
L_{ch}	flow channel length (m)
N_{turn}	number of turns in flow channel
P	pressure
Q	volume flow rate ($m^3\,s^{-1}$)
R	universal gas constant ($8.314\,kJ\,kmol^{-1}\,K^{-1}$)
R_0	outer diameter for U-turn of flow channel
Re	reynolds number
s	distance between flow channels (land width) (mm)
T	temperature (K)
$\mathbf{u}$	velocity vector ($m\,s^{-1}$)
V	average velocity ($m\,s^{-1}$)
w	flow channel width (mm)
W	bipolar plate effective width (m)

Greek letters

Δ	difference
δ_e	thickness of gas diffusion layer
μ	viscosity ($N\,s\,m^{-2}$)
ρ	density ($kg\,m^{-3}$)
ζ	stoichiometry

Subscripts

cell	fuel cell
e	electrode (gas diffusion layer)
f	friction
GDL	gas diffusion layer
inlet	value at the inlet of the flow channel
max	maximum value
min	minimum value
outlet	value at the outlet of the flow channel
turn	U-turn

drop, resulting in excellent cell performances. The gas diffusion layer (GDL) also has considerable effects on the flow distribution in a PEM fuel cell. The thickness, porosity, permeability and the wetting characteristics of the pores are most important parameters which define the characteristics of the GDL. The pores can be hydrophobic with optimal value of polytetrafluoreothylene (PTFE) [5] not to be congested with liquid water. Water flow in GDL is experimentally investigated for various thicknesses and pore sizes by Benziger et al. [6]. Paganin et al. [5] observed a performance decrement at higher current densities when the diffusion layer thickness is increased. The thickness of the GDL was optimized by a mathematical modeling in Inoue et al. [7] and by cell performance tests in Lee et al. [8] and Jordan et al. [9], with various GDL parameters such as porosity, permeability and thickness. A thin GDL with small porosity results in good electrical conductivity, however efficient mass transport requires large pores.

Multi-dimensional numerical simulations have been carried out to study the reactant transport and electrochemical reactions in a PEM fuel cell. Two-dimensional numerical analyses have been conducted along the flow direction by Hum and Li [10] and Chen et al. [11], and normal to the flow direction by Jeng et al. [12], among many others. In these works, the reactant transport was modeled including GDL on the assumption that the flow channel is straight and symmetrical to the boundary. Several three-dimensional simulations have been performed by Um and Wang [13], Hu et al. [14] and Hwang et al. [15] for the interdigitated flow channel. They reported that the flow through GDL enhances mass transport and improve the performance due to the enhanced reaction area. Most of numerical modelings and simulations, however, are based on symmetry considerations within the limited computational domains to reduce the computational costs [10–15]. Although such simplifications may be reasonable for simple reciprocating designs, e.g., parallel straight flow channels, it is not acceptable for the fuel cell with a long serpentine type flow channel. A typical serpentine flow channel has the cross section size in the order of $1\,mm^2$ or less and the length up to a few meters with many U-turns to fill the cell area on the bipolar plate as shown in Fig. 1. The pressure drop along the flow channel also results in a considerable pressure gradient across the GDL to the neighboring downstream channel due to much shorter distance. As a result, additional flow motion through GDL occurs, and is driven by the pressure gradient. This flow between the adjacent flow channels through the porous GDL has been referred to as flow cross over or cross leakage flow [16–25]. Convective flow motion through gas diffusion layer has been predicted in 2D [16,25] and 3D [6,7,17,22] numerical simulations for a PEM fuel cell with conventional serpentine flow channels with various emphases. The effect of cross flow on cell performance was investigated through cell performance test using GDL with distinctively different gas permeability [19]. Dohle et al. [20] obtained flow homogeneity in GDL through flow visualization to find optimal permeability value for best performance.

As a result of this cross leakage flow, (i) the flow rate (or pressure) at any cross section of the flow channel cannot be treated as a known boundary condition, except at the inlet and outlet, since it is strongly coupled with this cross leakage flow; (ii) the effect of the cross flow is substantial on the total pressure drop in a cell because the cross flow brings about enlarging effective flow area. For example, present experimental results revealed that the amount of pressure drop in the presence of cross flow is up to 80% smaller than that in the absence of cross flow for a typical PEM fuel cell of $100\,cm^2$ active cell area and 190 μm thick GDL with a single serpentine flow channel; (iii) the channel to channel symmetry, often used in CFD type simulation for the PEM fuel cell in order to reduce the computational domain, breaks down, as shown in ref. [16]. This symmetry breakdown requires the simulation of the entire cell instead of often employed in literature and a much-reduced domain ranging from half anode flow

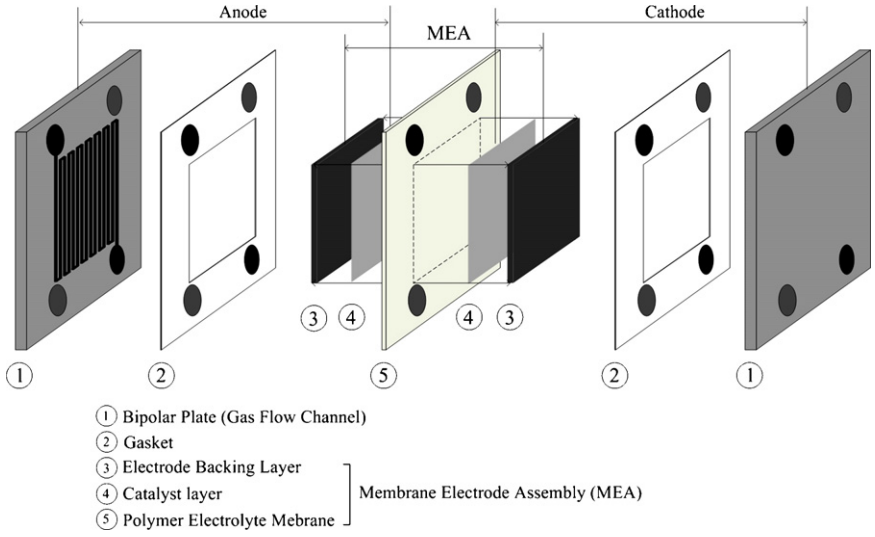

Fig. 1. Schematic of a polymer electrolyte fuel cell assembly.

channel to half cathode flow channel with membrane electrode assembly sandwiched in-between; (iv) the most important effect of the phenomenon perhaps lies in the fact that the cross leakage flow through the GDL creates the convection flow through the porous electrode structure, resulting in effective water removal from the porous electrode structure. The cross leakage flow is significant [26] in actual PEM fuel cells, and needs to be included in any PEM fuel cell analysis and simulation, although it has been often neglected in previous PEM fuel cell studies.

Therefore, the present study has been carried out to provide an experimental result documenting the degree of the cross flow effect on the reactant flow in a serpentine flow channel, and to provide a robust analysis on the cross leakage flow and its effects on flow distributions in a PEM fuel cell with a serpentine flow configuration. As pointed out early, three-dimensional numerical flow simulation of the entire flow channel, not a much-reduced domain, is necessary to capture the entire phenomenon. Hence, a three-dimensional numerical simulation has been performed covering the entire flow channel and GDL in a cell with the same physical dimensions and flow rates as the ones used in the experimental measurement. The effect of this cross leakage flow on the flow and pressure distributions has been analyzed for a wide range of flow conditions, as well as the permeability and thickness of the GDL. The numerical results are compared with the experimental measurements and good agreement is obtained.

2. Experimental setup

A PEM cell consists of a membrane electrolyte assembly (MEA) sandwiched between two bipolar plates as shown in Fig. 1. The gas diffusion layer (electrode backings), catalyst layer and polymer electrolyte membrane are referred to as MEA where current is produced. Fuel and oxidant are supplied to both sides of MEA through the flow channels on the bipolar plates producing electron in the anode catalyst layer and water in the cathode catalyst layer. The polymer electrolyte membrane con-

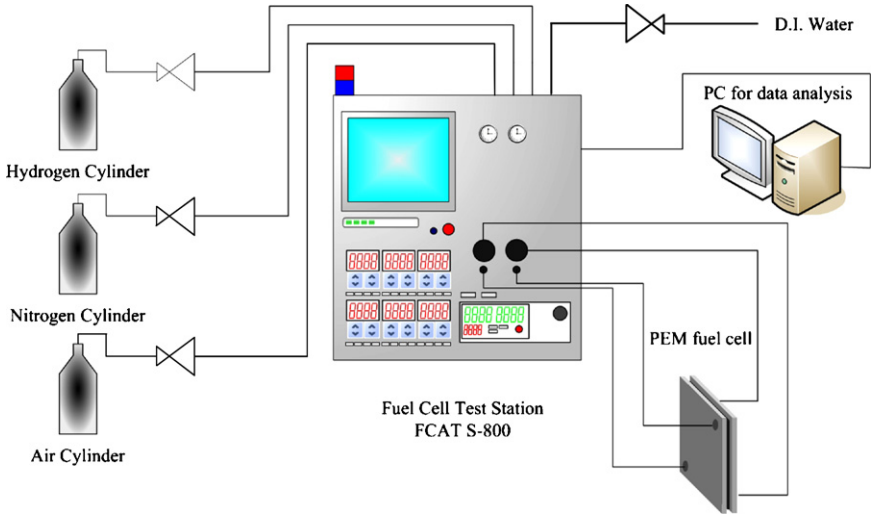

Fig. 2. Experimental setup.

Table 1
Dimensions and conditions in the present PEM fuel cell simulation

Parameter	Value
Bipolar plate	
Number of channel, N_{ch}	1
Number of U-turn, N_{turn}	50
Channel width, w (mm)	1.0
Land width, s (mm)	1.0
Channel depth, d (mm)	1.1
Channel length, l (m)	5.05
Channel hydraulic diameter, d_h (mm)	1.0476
Cell active area, A_c (cm^2)	100.1
Gas diffusion layer	
Outlet pressure, $P_{C,out}$ (atm)	1
Permeability, K (m^2)	10^{-13} to 10^{-6}
Porosity, ε	0.5
Thickness, δ_e (μm)	50–200
Cell general	
Assembling torque (lb in.$^{-1}$)	50
Flow rate velocity (m s^{-1})	3–30
Inlet humidity (%)	100
Temperature (°C)	20

ducts the proton produced by hydrogen oxidation to the cathode. Fig. 2 presents a schematic for the measurement of pressure drop in a PEM fuel cell. Measurement was carried out for the cathode side since the cross flow is more significant owing to the higher flow rate in cathode stream, although measurements for the anode side can be measured with the same apparatus. A Fuel Cell Automated Test Station (FCATS S-800, Hydrogenics Inc.) was used for the present experiment. The FCATS system consists of a gas supply and conditioning sub-system, electronic load box, and a computer based control interface which performs data acquisition as well, a detailed description of the FCATS is available elsewhere, e.g., [27]. The flow rate of the gas stream can be controlled within the ±1.0% of the full-scale flow (16,000 sccm). Using the technique of steam injection, filtered de-ionized water is supplied to the gas streams to control the relative humidity. One hundred percent relative humidity air was employed in all of the experiments. Single cell test fixtures with active areas of 100.1 cm^2 were assembled for testing using MEAs manufactured by Ion Power Inc. All parameters including flow conditions and dimensions are given in Table 1.

The pressure drop from the channel inlet to the channel outlet was measured for two different conditions: in the presence and absence of cross flow. For the latter case, the test cell was assembled with an impermeable film in place of MEA. Test cells were checked for gas leakage from the cell peripherals after the cell assembly and before the actual experimental measurements. Then before each measurement to be conducted, the cell assembly was pressurized up to 150 kPa with the channel exit closed. The cell was considered to have no leakage if the pressure was sustained for 1 min. Pressure data was stored with flow conditions after the system reached a steady-state which was typically within 1 min after a new flow rate was set.

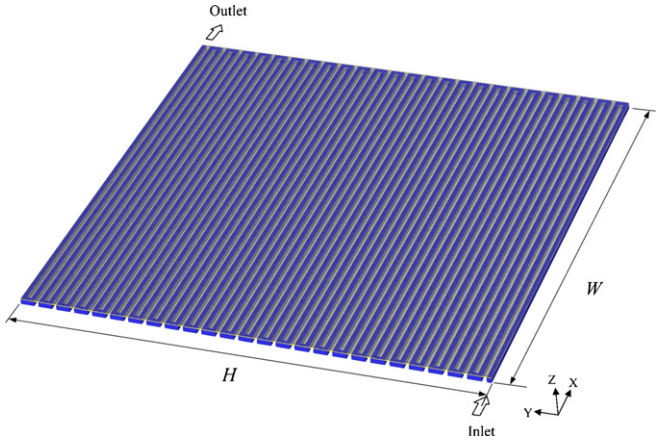

Fig. 3. A geometrical model of the flow channel and electrode backing layer.

3. Numerical simulation

The computational domain for the present numerical simulation includes a GDL and a serpentine flow channel, which is grooved on the bipolar plate, as shown in Figs. 3 and 4. Fully humidified air is considered as the reactant gas mixture in the cathode side and the following assumptions are made for the present simulations:

(1) The gas mixture behaves like ideal gas, and is incompressible.
(2) The GDL is considered to be isotropic porous media with constant porosity.
(3) Flow is isothermal and laminar.
(4) Water exists as a vapor only, hence only single-phase flow is considered.

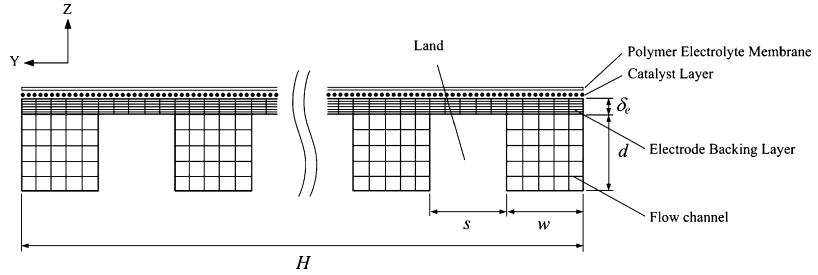

Fig. 4. The details of computational domain and grid arrangement for numerical simulation.

Fig. 4 shows a typical three-dimensional structured grid for the flow channel and GDL used for the present numerical analysis. In the flow channel, the flow field is obtained by solving the steady-state Navier–Stokes equations:

$$\nabla \cdot (\rho \mathbf{u}) = 0 \tag{1}$$

$$\nabla \cdot (\rho \mathbf{u}\mathbf{u}) = -\nabla P + \mu \nabla^2 \mathbf{u} \tag{2}$$

where ρ is density, $\mathbf{u}$ the velocity, P the pressure and μ is the viscosity. The pressure drop in the GDL is proportional to velocity if the flow is laminar. This can be modeled by the addition of a viscous loss term according to Darcy's law [16] such that the governing equations for the GDL becomes:

$$\nabla \cdot (\rho \mathbf{u}) = 0 \tag{3}$$

$$\nabla \cdot \left(\rho \frac{\mathbf{u}\mathbf{u}}{\varepsilon}\right) = -\varepsilon \nabla P + \mu \nabla^2 \mathbf{u} - \frac{\mu}{K}\varepsilon \mathbf{u} \tag{4}$$

where ε is the porosity and K is the permeability of GDL. Since the pressure and Darcy's terms are dominant over other terms Eq. (4) may be simplified in GDL, as often used in fuel cell analysis in literature:

$$\nabla P = -\frac{\mu}{K}\mathbf{u} \tag{5}$$

where $\mathbf{u}$ is the superficial velocity in the porous medium. The constant pressure was given at the exit of the flow channel as boundary condition while the inlet boundary condition was assumed to have constant velocity. All other surfaces except the inlet and the outlet are assumed as no slip walls.

The conservation of mass and momentum equations were discretized using the finite volume method (second order upwind scheme) and solved by the commercial software FLUENT 6.0. It costs large amount of computational resource to simulate the entire flow channel with GDL since the flow channel and GDL has high aspect ratio of length to thickness. The length of the flow channel is 5.05 m with 50 U-turns on 10 cm × 10 cm of cell active area while the thickness of the channel and GDL are 1 mm and 50–200 μm, respectively. At least more than 5 grid points were given for the channel width and the GDL thickness, which is equivalent to 200 μm for flow channel and 10–40 μm for the GDL, respectively. The number of the computational cells in the flow channel may seem a bit low at the first look, however, it is reasonably sufficient for the present purpose. Since this is validated by doubling the number of computational cells around the bend region. Secondly, the significant cross flow shown in this study that injects the fluid into and out of the supposed secondary flow vortices zone around the channel bend areas weakens the secondary flow significantly. Similarly, Shimpalee et al. [22] used 6 computational cells for the flow channel in a related simulation. A total of 1.5 million grid points have been generated for the entire computational domain consisting of the flow channel and GDL. The Eqs. (1)–(4) were solved iteratively and the solution was considered to be convergent when the relative error in each field between two consecutive iterations was less than 10^{-4}. Each case took about 7–10 h iteration time using the personal computer equipped with dual CPUs and 4 Giga-byte of main memory.

Table 2
Bend head loss correlations [29]

Configuration	Correlations
Bending 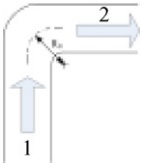	$\Delta P_{\text{bend}} = k\frac{\rho V^2}{2}$
	$k = k_{\text{loc}} + k_{\text{fr}}$
	$k_{\text{loc}} = \frac{0.21}{(R_0/d_{\text{h}})^{0.25}}$ (90° bend, square duct)
	$k_{\text{fr}} = 0.0175\frac{R_0}{d_{\text{h}}}\delta\lambda$ (δ in degrees)
	$\lambda = 32\left(Re_{d_{\text{h}}}\sqrt{\frac{2R_0}{d_{\text{h}}}}\right)^{-(2/3)}$ (Laminar)

$R_0 \approx 1.2 d_{\text{h}}$ in the present design.

4. Pressure drop through engineering correlations

The experimentally measured pressure drops from the channel inlet to the channel outlet without GDL (impermeable walls) were also compared with the pressure drops determined by the Darcy–Weisbach's correlation [28] in this study. The pressure drop caused by frictional loss along the flow channel can be estimated as from:

$$\Delta P = C_{\text{f}}\frac{L}{d_{\text{h}}}\frac{\rho V^2}{2} \tag{6}$$

where C_{f} is the friction coefficient, L the length of the flow path, d_{h} the hydraulic diameter of the flow path, ρ the fluid average density, and V is the flow speed. The friction coefficient depending on the flow condition is expressed in terms of Reynolds number [28]:

$$C_{\text{f}} = \begin{cases} \dfrac{C_{\text{l}}}{Re_{d_{\text{h}}}}, & \text{Laminar}: \ Re < 2 \times 10^3 \\ \dfrac{0.316}{Re_{d_{\text{h}}}^{1/4}}, & \text{Turbulent}: \ 4 \times 10^3 < Re < 10^5 \end{cases} \tag{7}$$

where C_{l} is 56.9 for the laminar flow in a square flow channel [28]. The Reynolds number is defined based on the hydraulic diameter of the flow path,

$$Re = \frac{\rho V d_{\text{h}}}{\mu} \tag{8}$$

where μ represents average viscosity in the flow. Since the flow condition in flow channel is mostly laminar in the present study Eq. (6) can be reduced as:

$$\Delta P = C_{\text{l}}\frac{\mu L}{2d_{\text{h}}^2}V \tag{9}$$

The minor losses associated with the bending of the flow channels are included in the estimation of the total pressure drop in the flow channel. Table 2 lists the minor loss correlations used in this study [29].

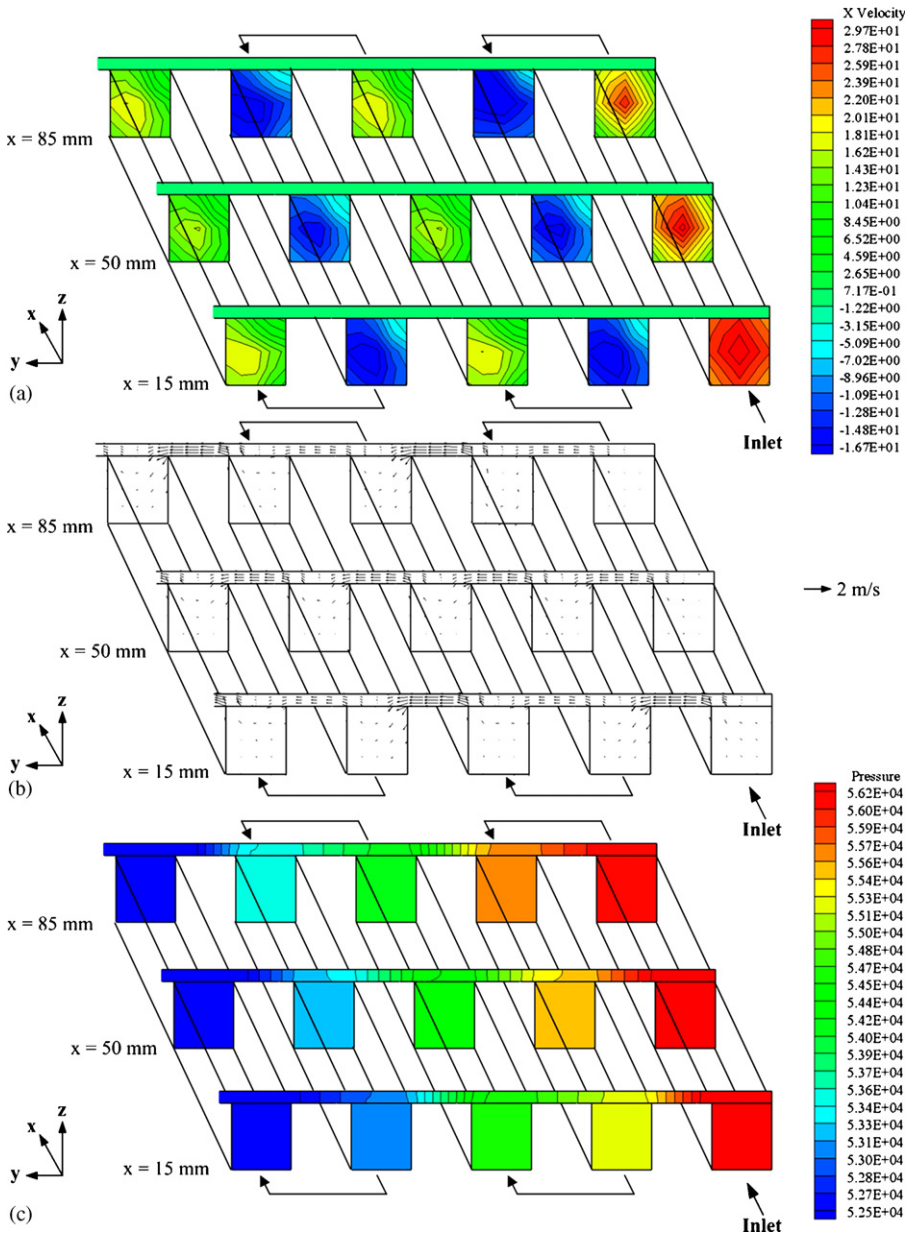

Fig. 5. Flow structure in the first five flow channels and gas diffusion layer at several axial positions: (a) contour plot for the x-axial flow velocity, (b) two-dimensional velocity vectors (y and z component), (c) static pressure distribution. $V_{inlet} = 27\ m\ s^{-1}$, $\delta_e = 200\ \mu m$, $K = 1.76 \times 10^{-11}\ m^2$ (K value is taken from [19]).

5. Results and discussion

5.1. Characteristics of cross flow

The GDL, as porous electrodes for the anode and cathode side, is generally made of a porous carbon paper or carbon cloth, with a typical thickness in the range of 50–200 μm in a PEM fuel cell. The porous structure of the electrodes enables the effective diffusion of the reactant gases to the catalyst layer in the MEA increasing the effective surface area available for the electrochemical reactions. The porous electrode also assists in water management by allowing the appropriate amount of water vapor to enter the MEA and humidify the polymer electrolyte. Although there exists a large amount of drag caused by porous structure the reactant transport can be driven not only by concentration gradient but also by pressure gradient in GDL.

The flow structures for a typical serpentine flow channel and thin diffusion layer are shown in Fig. 5 in which (a), (b) and (c) represent the magnitude of axial velocity (x-component), two-dimensional velocity vectors (consisted of y- and z-component) and static pressure distribution at the three axial positions of 15, 50 and 85 mm, respectively, for the first five channels from the channel inlet. Fig. 5(a) indicates that the axial velocity develops from the channel inlet and becomes developed gradually in the downstream direction with the maximum velocity near the center for the first channel. The axial velocity decreases drastically close to the GDL due to the substantial drag caused by the low permeability of the GDL. It is interesting to observe that the max-

imum velocity as well as the cross sectional velocity distribution of the flow are skewed considerably in the second flow channel towards the downstream channel direction due to the cross flow from the upstream as well as to the downstream channels. It is seen that the degree of skew is increased for the third, fourth and fifth channels, or the successive downstream channels, because of the cumulative effect of the cross flow through the GDL.

The flow structure in GDL is characterized by the two-dimensional velocity vector consisting of y- and z-component in Fig. 5(b). The cross flow velocity to the downstream channel decreases as the flow approaches the U-turn (the end of the channel) where the pressure difference between the two adjacent channels is the smallest. In contrast, the velocity from the upstream channel increases as the flow approaches the U-turn owing to increasing pressure gradient across the GDL. The static pressure distribution shown in Fig. 5(c) indicates that the pressure in the flow channel decreases downstream and that the lowest pressure gradient in the GDL occurs with the upstream channel before the U-turn and the highest pressure gradient with respect to the downstream channel occurs after the U-turn. It is also noticed that the pressure gradient in the channel area is much smaller than that in the GDL so that no pressure contour appears in Fig. 5(c) for the channel area. However, the pressure contour in the GDL is almost vertical in the area between the channels, indicating that the cross flow is from the upstream to the downstream channel with velocity almost parallel with the thickness of the GDL. However, the pressure contour in the GDL above the channel area is inclined, suggesting the velocity is also inclined in this area, similar to the previous results [16].

Fig. 6 shows the average pressure in the GDL for various values of the GDL permeability and thickness which are the two major parameters affecting the amount and characteristics of the cross flow. As implied by Eq. (4), the permeability of the GDL has a direct and major impact on the cross flow, while the porosity will influence the cross flow indirectly through its relation with the permeability. The average pressure shown in Fig. 6 was obtained based on the two-dimensional pressure data set on the plane $x = 50$ mm for the GDL only and averaged for the same y positions. It is seen that pressure drops almost linearly in the y direction (in the cross channel direction) for all cases however the amount of pressure drop is considerably affected by the value of permeability in Fig. 6(a) and the thickness of GDL in Fig. 6(b). It is clear that the pressure drop in the cross channel direction, hence the cross flow between successive channels, is governed mainly by the permeability and thickness of the GDL.

Fig. 7 provides four pathlines for the four fluid particles initially located at four different vertical locations at the inlet flow channel cross section shown in Fig. 7(c). Fig. 7(a) shows the results for the GDL permeability of 10^{-9} m^2, while Fig. 7(b) for the permeability of 10^{-10} m^2. It is seen that the fluid particle a, being located on the top location, is the first being transported into the next flow channel by the cross flow, while the fluid particle d, being at the lowest position of the four investigated, travels the longest distance in the original flow channel before

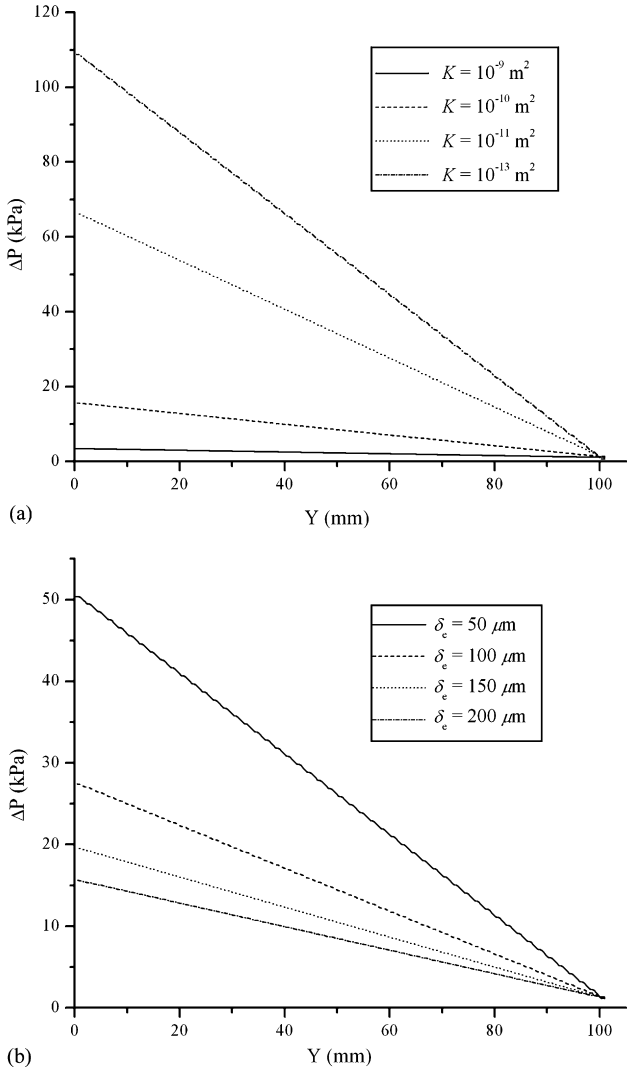

Fig. 6. Average pressure in the gas diffusion layer on the plane $X = 50$ mm in the y-direction: (a) $\delta_e = 200$ μm, (b) $K = 10^{-10}$ m^2. The vertical coordinate ΔP represents that the local average pressure is with respect to the pressure at the outlet.

being transported to the next channel via the GDL by the cross flow. The left figures in Fig. 7(a and b) indicate that the fluid particles in the second, third, and further downstream channels are transported down the flow channel in the main direction of the channel flow before the cross flow takes them to the next downstream channels. However, the face view of the flow particle trajectories shown in the right figures in Fig. 7(a and b) shows a striking difference. For the larger permeability GDL shown in Fig. 7(a), the fluid particles move from channel to channel by the strong cross flow without any noticeable convection effect of the main flow in the channels, except the first and last few channels near the inlet and exit. On the other hand, for the lower permeability results shown in Fig. 7(b), a much weaker cross flow results in the fluid particle trajectory significantly affected by the main flow in the flow channels. This highlights the complexities of the cross flow characteristics for different GDLs with various values of the permeability. Similar behavior can be observed as well for different thicknesses of the GDL as well.

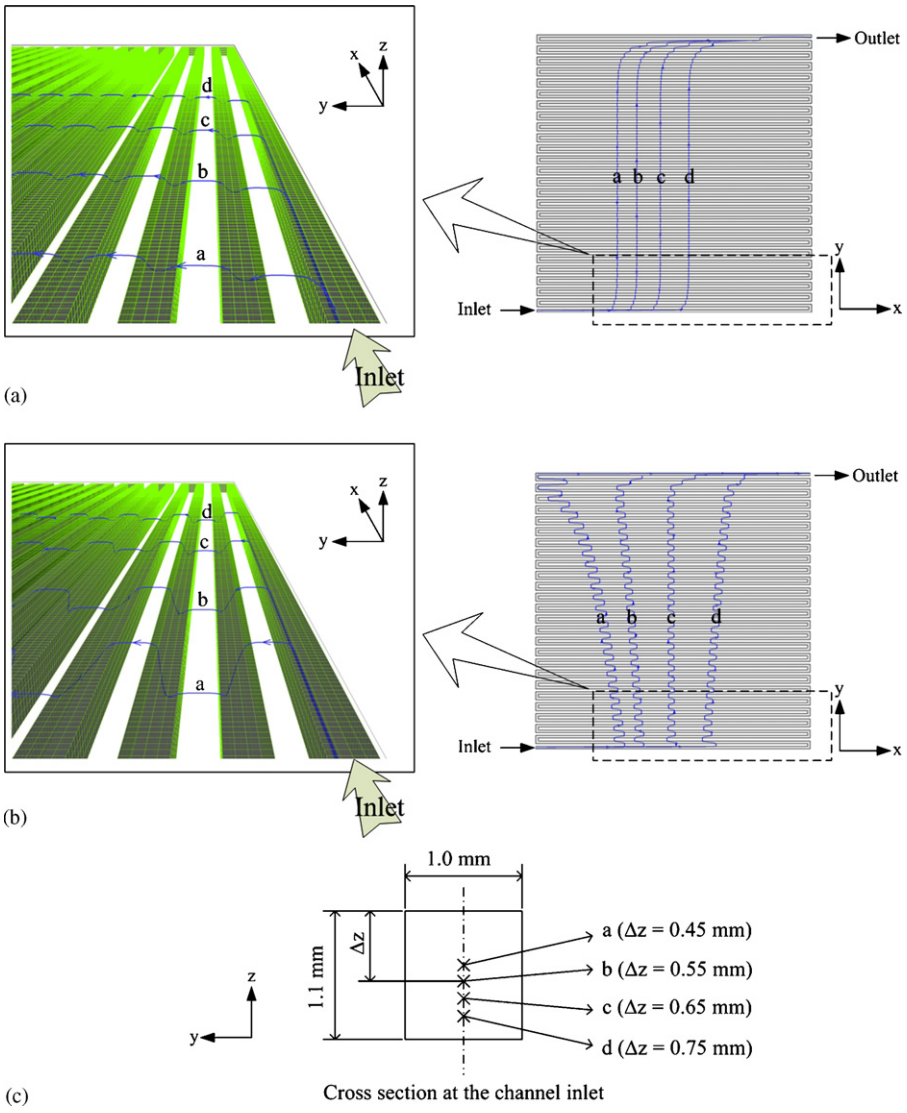

Fig. 7. Pathlines illustrating the cross flows for four fluid particles starting from the four different start positions at the inlet of the flow channel: $\delta_e = 200\,\mu m$, (a) $K = 10^{-9}\,m^2$, (b) $K = 10^{-10}\,m^2$, (c) the position of the four fluid particles at the channel inlet cross section.

5.2. *Quantity of cross flow; experimental measurement and numerical simulation*

The transport of reactant gas and water in GDL is the most critical aspect for interdigitated flow configurations [13–15] since no flow path is connected to the exit. Although the cross flow in PEM fuel cells with serpentine flow configurations have been reported before [16–18,22], its effect has been largely unaccounted for in most of designs and numerical modelings; for example, the amount of pressure drop was simply calculated using Eq. (6) including minor losses, assuming all the flow is in the channel. The amount of pressure drop in an actual fuel cell assembly has been measured for various flow conditions and compared with numerical results in Fig. 8. The PEM fuel cell for the present study has an active area of 100.1 cm^2 with one single serpentine flow channel (1.0 mm width × 1.1 mm depth) and the thickness of the GDL was measured to be 190 μm when the cell was assembled. Physical dimensions and flow conditions are listed in Table 1. The experimental results are given in symbols. It is seen that the pressure drop from the channel inlet to the channel outlet increases as the inlet Reynolds number is increased for both cases with the MEA sandwiched between the two flow plates (marked as "with GDL") and with an impermeable plate in between the two flow plates (marked as "without GDL"). It should be emphasized that the difference between the amount of pressure drop for two cases with and without the MEA is significantly large, as large as up to 80% of the pressure drop for the case without the MEA.

In order to confirm that the significant difference in the pressure drop is indeed due to the cross flow phenomena described early, the results from both the three-dimensional numerical simulation and the engineering correlation, Eq. (6), including minor losses listed in Table 2, are also plotted in Fig. 8. It is observed that the results from the empirical correlation and the present numerical simulation are in reasonable agreement with the experimental measurements for the case without the MEA.

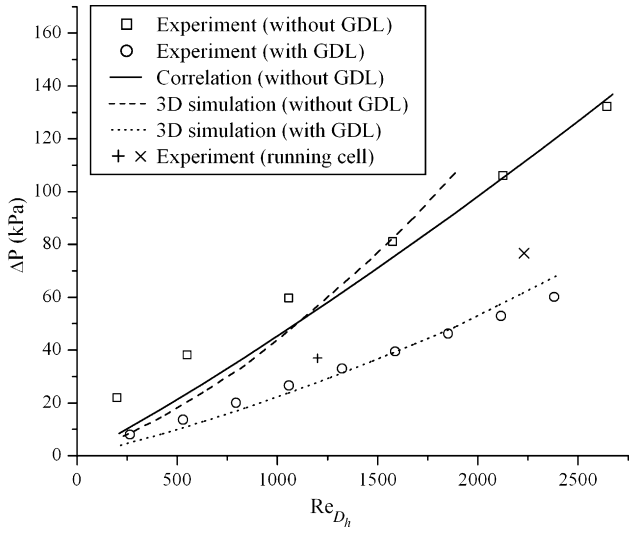

Fig. 8. Comparison of the amount of pressure drop vs. the Reynolds number at the channel inlet with and without gas diffusion layer (GDL): $\delta_e = 190\ \mu m$ and $K = 1.76 \times 10^{-11}\ m^2$ used in the 3D simulation; experimental data from actually operating PEM fuel cell at the current density of 0.2 (+) and 0.4 A cm^{-2} (×), stoichiometry (humidified air, cathode stream) of 3.0, operating temperature of 80 °C; all physical dimensions of the cell are kept the same as those given in Table 1.

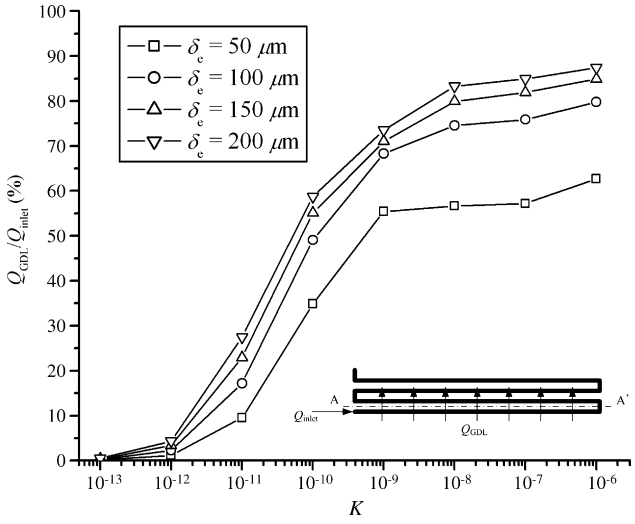

Fig. 9. Ratio of the volume flow rate for the cross flow through the gas diffusion layer to the inlet total flow rate Q_{inlet} for various permeability values: $Q_{inlet} = 3.08 \times 10^{-5}\ m^3\ s^{-1}$, A–A′ is the surface only in the gas diffusion layer through which the cross flow rate Q_{GDL} is calculated.

However, some difference exists at lower Reynolds numbers at the channel inlet. It is seen that for the low inlet Reynolds numbers the pressure drop estimated from the empirical correlation and numerical simulation agree with each other very well, although they both deviate from the experimental results with similar differences – this difference arises because in the experiments when the flow channel plates are assembled with the impermeable transparency replacing the MEA in the middle, the transparency bulged into the flow channel area resulting in smaller flow channel sizes, hence higher pressure drop in the measured data. As the absolute pressure in the channel increases with the flow rate since the channel exit pressure is kept constant during the experiments, the transparency is being pushed back, the bulging effect is reduced and the prediction from both empirical and numerical results agree better with the experimental results as the flow rate or the inlet Reynolds number is increased.

Fig. 8 also indicates that the experimental results for the case with the MEA are substantially lower compared to the case without the MEA, the present three-dimensional numerical simulation considering the cross flow phenomena again yields results that compare very well with the experimental results for the case with the MEA. Therefore, the substantial difference in the pressure drop with and without the MEA can be attributed to the effect of cross flow phenomena described in this study. Also in Fig. 8, two measurements are shown for the cell in operation at the current density of 0.25 and 0.5 A cm^{-2}, corresponding to the cathode stoichiometry of 2. The water produced from reaction could be mostly in liquid form since the cathode inlet stream is saturated with water vapor. If the effect of the diffusion and electroosmotic drag is neglected, the resultant pressure drop for the running cell could be lower than that for the case with MEA due to the consumption of the oxygen. However measured values for the running cell are actually higher than the result for the case with the MEA in Fig. 8. This implies that liquid water might have existed inside the unit cell, that blocks the reactant flow, whether in the flow channel or in the GDL, resulting into higher pressure drop in the cell.

From the preceding discussion, the effect of cross flow can be summarized as follows: The amount of pressure drop for an actual PEM fuel cell is significantly lower than the case without cross flow being considered. This lower pressure drop results in lower concentration gradient in cell with less pumping energy requirement. The reaction area can be enhanced by cross flow, which will bring about better performance, similarly to the cases studied for interdigitated flow configurations [13–15]. Further, the cross flow through the GDL could be an effective mechanism for the removal of water accumulated in the GDL. These factors together contribute to the better performance of PEM fuel cells using serpentine flow channel layouts, a fact that is well known for industrial PEM fuel cell developers and experimentalists [3].

The amount of cross flow is quantified as the volume flux through the first land area (between the first and second flow channel) and the results are presented as a relative amount to the total inlet flow rate in Fig. 9. As indicated previously, the cross flow is affected significantly by the permeability and thickness of the GDL. Permeability is a measure of the ability of a material (typically a porous medium) to transmit fluids through it. A typical value of the permeability is within a range between 10^{-12} and $10^{-10}\ m^2$ for the GDL in a PEM fuel cell [6,15,30] while the thickness of the GDL may vary according to the designs and manufacturers. The amount of cross flow is considerable throughout the typical range of permeability and becomes dominant for the permeability greater than $10^{-10}\ m^2$. For instance, the amount of cross flow is more than 50% of the total inlet flow rate for the GDL thicker than 100 μm. For the MEA investigated experimentally in this study, corresponding to the results shown

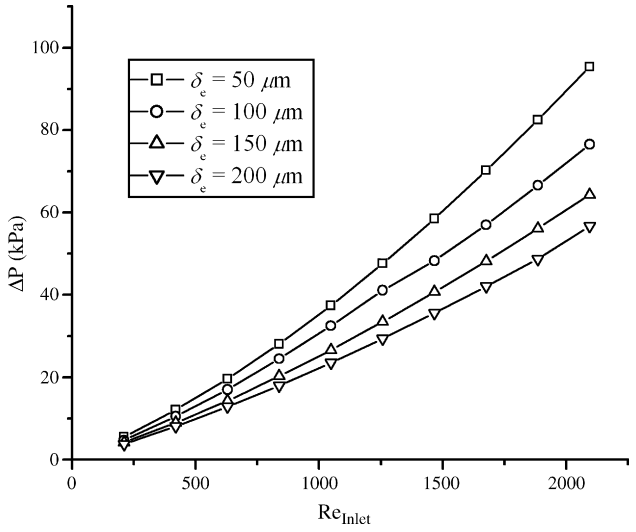

Fig. 10. The total pressure drop from the flow channel inlet to the channel outlet for different thicknesses of the gas diffusion layer; $K = 1.76 \times 10^{-11}$ m^2 taken from [19].

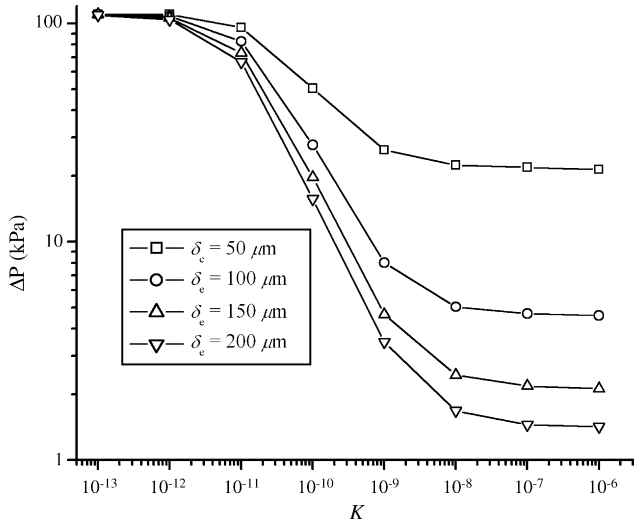

Fig. 11. The total pressure drop from the flow channel inlet to the channel outlet for various permeability values of the gas diffusion layer: $V_{inlet} = 27$ m s^{-1}.

in Fig. 8, as much as 40% of the inlet flow does not follow the flow channel path, rather it crosses the land area through the GDL between the first and the second flow channel. Since the cathode GDL is most susceptible to liquid water flooding, this strong cross flow, coupled with a small width of the land area between the successive channels, would be beneficial for the removal of liquid water in the cathode GDL under the land area.

5.3. Effects of permeability and thickness of GDL on the pressure drop

It has been shown in the previous sections that the thickness and properties of GDL such as permeability are governing parameters influencing the cross flow in a PEM fuel cell with serpentine flow channels. The thickness of GDL can be measured after the cell is assembled, however porosity and permeability may not be known precisely for GDL as indicated previously. The permeability values for the GDL is quite different in literature while the value for the porosity is typically in the range of 0.3–0.5 as noticed from refs. [12–15]. The strength of the flow resistance in the GDL, as shown in Eq. (4) or (5), is mainly influenced by the value of permeability and velocity. Therefore, simulation has been performed in a wide range of permeability and flow rate to investigate their effects on the amount of pressure drop in a cell. Fig. 10 shows the total pressure drop from the channel inlet to the channel outlet increases as the inlet Reynolds number is increased for all the GDL thicknesses investigated. However, the pressure drop for thicker GDLs is smaller due to a larger amount of cross flow through the GDL as shown previously in Fig. 9. The rate of increase for the pressure drop against the inlet flow rate becomes larger for thinner GDLs, attributable to the fact that the amount of the cross flow does not increase correspondingly with the inlet flow rate.

Fig. 11 shows the total pressure drop for a wide range of permeability values for various thicknesses of GDL. It is seen that the pressure drop is larger for thinner GDL due to a weaker cross flow through such GDLs, and it decreases as the value of permeability is increased. However, the major decrement occurs within the range of permeability between 10^{-12} and 10^{-8} m^2. The GDL behaves more like an impermeable wall for permeability lower than 10^{-12} m^2 so that the pressure drop becomes almost identical for all different GDL thicknesses, and is equivalent to the pressure drop without GDL. On the other hand, the GDL provides additional flow path for larger values of permeability, so that beyond the permeability value of 10^{-8} m^2 the pressure drop becomes almost independent of the permeability values, and is inversely proportional to the GDL thickness.

6. Conclusions

In this study the characteristics and effect of cross flow through the porous electrode structure between two adjacent flow channels have been investigated numerically and experimentally for a PEM fuel cell with a serpentine flow channel layout. Experimental measurements revealed that the total pressure drop from the channel inlet to the channel outlet in a PEM fuel cell is reduced substantially when compared with the case without the gas diffusion layer (that is, impermeable wall), and the amount of reduction can be as much as up to 80% for low flow conditions, although the percentage of reduction is decreased as the channel inlet Reynolds number is increased. Three-dimensional numerical simulation indicates that permeability and thickness of the gas diffusion layer are the two most important parameters influencing the cross flow and the resultant pressure drops. The total pressure drop is reduced for larger values of the permeability and thickness of the gas diffusion layer, and significant reduction occurs within the permeability range of 10^{-12} and 10^{-8} m^2. For the PEM fuel cell investigated in this study, a significant amount of the cross flow through the gas diffusion layer occurs, about 40% of the flow rate at the channel inlet. The present study suggests that cross flow through the gas diffusion layer between the adjacent flow channels is substantial,

and this strong convection current would help bring the reactant gas to the reaction sites and drive the liquid water out of the electrode structure for effective water management, hence partially responsible for the good performance of PEM fuel cells with serpentine flow channels. As a result, the effect of cross flow should be included for the analysis, simulation, design, operation, and performance optimization of practical PEM fuel cells.

Acknowledgment

This work was supported by AUTO21, the Network of Centers of Excellence, Canada.

References

[1] D.S. Watkins, K.W. Dircks, D.G. Epp. US Patent no. 5,108,849 (1992).
[2] D.S. Watkins, K.W. Dircks, D.G. Epp. US Patent no. 4,988,583 (1991).
[3] X. Li, Principles of Fuel Cells, Taylor & Francis, New York, 2005.
[4] X. Li, I. Sabir, Int. J. Hydrogen Energy. 30 (4) (2005) 359–371.
[5] V.A. Paganin, E.A. Ticcianelli, E.R. Gonzalez, J. Appl. Electrochem. 26 (3) (1996) 297.
[6] J. Benziger, J. Nehlsen, D. Blackwell, T. Brennan, J. Itescu, J. Membrane Sci. 261 (2005) 98–106.
[7] G. Inoue, Y. Matsukuma, M. Minemoto, J. Power Sources 154 (2006) 8–17.
[8] H. Lee, J. Park, D. Kim, T. Lee, J. Power Sources 131 (2004) 200–206.
[9] L. Jordan, A. Shukla, T. Beehrsing, N. Avery, B. Muddle, M. Forsyth, J. Power Sources (2000) 250–254.
[10] B. Hum, X. Li, J. Appl. Electrochem. 34 (2004) 205–215.
[11] F. Chen, Y. Wen, H. Chu, W. Yan, C. Soong, J. Power Sources 128 (2004) 125–134.
[12] K. Jeng, S. Lee, G. Tsai, C. Wang, J. Power Sources 138 (2004) 41–50.
[13] S. Um, C. Wang, J. Power Sources 125 (2004) 40–51.
[14] G. Hu, J. Fan, S. Chen, Y. Liu, K. Cen, J. Power Sources 136 (2004) 1–9.
[15] J. Hwang, C. Chen, R. Savinell, C. Liu, J. Wainright, J. Appl. Electrochem. 34 (2004) 217–224.
[16] T. Kanezaki, X. Li, J.J. Baschuk, Cross leakage flow between adjacent flow channels in PEM fuel cells, J. Power Sources 162 (2006) 415–425.
[17] S. Dutta, S. Shimpalee, J.W. Van Zee, Int. J. Heat Mass Transf. 44 (2001) 2029–2042.
[18] J.G. Pharoah, J. Power Sources 144 (2005) 77–82.
[19] M.V. Williams, H.R. Kunz, J.M. Fenton, J. Electrochem. Soc. 151 (2004) A1617–A1627.
[20] H. Dohle, R. Jung, N. Kimiaie, J. Mergel, M. Muller, J. Power Sources 124 (2003) 371–384.
[21] P.T. Nguyen, T. Berning, N. Djilali, J. Power Sources 130 (2004) 149–157.
[22] S. Shimpalee, W.k. Lee, J.W. Van Zee, H. Naeri-Neshat, J. Power Sources 156 (2006) 355–368.
[23] P.H. Oosthuizen, L. Sun, K.B. Mcauley, Appl. Therm. Eng. 25 (2005) 1083–1096.
[24] Y. Wang, C.Y. Wang, J. Power Sources 147 (2005) 148–161.
[25] W. Sun, B.A. Peppley, K. Karan, J. Power Sources 144 (2005) 42–53.
[26] I. Sabir, Experimental investigation of proton exchange membrane fuel cell, MASc Thesis, University of Waterloo, March 2005.
[27] A. Mughal, X. Li, Int. J. Environ. Stud. 63 (2006) 377–389.
[28] F. White, Fluid Mechanics, third ed., McGraw Hill, 1994.
[29] I. Idelchik, Handbook of Hydraulic Resistance, third ed., CRC Press, Boca Raton, 1994.
[30] V. Gurau, H. Liu, S. Kakac, AIChE J. 44 (11) (1998) 2410–2422.